



Synthesis of novel $\text{MnCo}_2\text{O}_4/\text{NaY}$ zeolite nanocomposite adsorbent and its performance for Sr^{2+} ions removal from drinking water

Meysam Sadeghi¹ · Sina Yekta² · Daryoush Mirzaei¹ · Abedin Zabardasti¹ · Saeid Farhadi¹

Received: 3 August 2018 / Accepted: 29 November 2018 / Published online: 3 December 2018
© Springer Nature B.V. 2018

Abstract

The present study describes the effective performance of $\text{MnCo}_2\text{O}_4/\text{NaY}$ zeolite (MnCo_2O_4 : 18.7 wt%) as a novel nanocomposite adsorbent for the removal of Sr^{2+} ions from drinking water of Tehran city. The reactions were all carried out under pre-organized optimized conditions and the subsequent monitoring was accomplished via the ultra-low level liquid scintillation counting (LSC) analysis. The characterization study of samples was carried out using scanning electron microscope, energy dispersive X-ray, atomic force microscope, powder X-ray diffraction and Fourier-transform infrared spectroscopy. Multiple experimental conditions including adsorbent dose, pH, adsorbent type and contact time were applied for the adsorption-removal process of Sr^{2+} ions by the $\text{MnCo}_2\text{O}_4/\text{NaY}$ nanocomposite adsorbent. The results from LSC concluded that Sr^{2+} was operatively adsorbed on the nanocomposite surface active sites after 180 min at room temperature with a yield more than 95%. The reaction kinetic data was precisely studied by employing pseudo-first and second-orders, intra particle diffusion and Elovich models. The adsorption kinetics was found to fit the pseudo-second-order model. Moreover, the investigation of the thermodynamic parameters such as ΔG^0 , ΔH^0 and ΔS^0 , specified that adsorption procedure of Sr^{2+} was spontaneous and expresses a physic-chemical adsorption characteristics and exothermic feature of the adsorption reaction. The sequential experiments of reproducibility for the synthesized nanocomposite against Sr^{2+} ions showed removal efficiency of more than 91% for all those cycles.

Keywords $\text{MnCo}_2\text{O}_4/\text{NaY}$ · Sr^{2+} ions · Removal · Kinetic · Thermodynamic

Introduction

Customarily, the radionuclides including natural and anthropogenic can be found in the surrounding environment. The natural radioactivity is referred to the radionuclides with considerably high half-lives originated historically from the formation of the planet earth [1]. On the other hand, the anthropogenic radionuclides are known as the artificial radioactivity sources that can be introduced to the environment through various path ways such as accidents in nuclear power plants leading to leaked/released radionuclides, worldwide fallout resulting from atmospheric weapons tests, plants for used fuel reprocessing, the large volumes of radiotoxic liquid

wastes generated from radiochemical laboratories and short-lived nuclides from the production of radioisotopes for several applications. Strontium-90 (^{90}Sr) is recognized as pure β -emitter ($T_{1/2} = 28.8$ year) and as this radionuclide decays, it emits radiation and ^{90}Y appears, which in turn decays to stable zirconium (^{90}Zr) [2]. ^{90}Sr can be directly measured by radiometric methods namely gas flow GM counting and liquid scintillation counting. Further, ^{90}Y known as the daughter of ^{90}Sr which is also pure β -emitter with a short half-life of 64 h can be usually seen as a twin along with ^{90}Sr spectrum attained from above noted measurement techniques [3]. Furthermore, ^{90}Sr is as one of the serious hazardous components of nuclear wastes. The nuclear fission of uranium and plutonium in nuclear reactors and also nuclear weapons are common offspring to create ^{90}Sr as a major by-product. Besides, unconfined nuclear weapon tests and unpredicted events and accidents in different nuclear power plants around the globe are always of significant concern for researchers and radioactivity monitoring laboratories/agencies. For instance, in 1950s and 1960s, great amounts

✉ Meysam Sadeghi
meysamsadeghi1177@gmail.com

¹ Department of Chemistry, Lorestan University, Khorramabad, Iran

² Department of Chemistry, Payame Noor University (PNU), Tehran, Iran

of ^{90}Sr were released and dispersed worldwide during atmospheric nuclear weapons tests. In addition, on April 26, 1986 the shocking outburst at the Chernobyl nuclear power plant [4] caused a large mass of ^{90}Sr into the environment and the Soviet Republics was strictly affected via deposition a great amount of ^{90}Sr . The remaining was scattered as fallout across Northern Europe and whole world. On March 11, 2011 a seaquake happened on the east side of Japan caused a hideous tsunami of 14 m height. Nevertheless, the nuclear power plants at the Fukushima sites were hit by a tsunami waves. The nuclear power plants at both Fukushima sites were just 10 m over sea level and the emergency generators were not secured versus such unpredicted cataclysm and the generators were flushed by water and failed eventually [5]. Considering the environmental aspect, ^{90}Sr deposits majorly by rain or other possible precipitation and would be available to plants by soil uptake process. Thus, it is not beyond the expectations for ^{90}Sr to effectively transpire into the human being food chain. After entrance through the body, it imbibes by gastrointestinal system and due to its chemical resemblance to calcium, concentrates in the bones and teeth. After its ingestion, about 70–80% of ^{90}Sr passes through the body and urine. The other remaining of 20–30% will be absorbed and deposited in the bone tissues. Also, about 1% is dispersed among the extracellular fluid, blood volume, surface of the bone and soft tissue, where it may remain and decay or possibly expelled. The murderous radiation effects of ^{90}Sr in the body include the disorder of new cells production, bone cancer, cancer of the soft tissue conjunct to the bone, leukemia and death [2]. Therefore, the removal of long-lived radionuclides from nuclear waste media should be taken into account in nuclear waste management. The physico-chemical processes such as coagulation, co-precipitation, solvent extraction, ion exchange, electrochemical processes and membrane processes [6] are commonly used for removal of radionuclides including ^{90}Sr from radioactive waste solutions [7]. Moreover, in the recent years there has been an increase in the utilization of different compositions of metal oxide nanoparticles and zeolites to eliminate the radioactive pollutants [8, 9]. The mixed transition metal oxides (MTMOs) with spinel structure are attracting increasing interest due to their potential applications in industry and research [10–15]. Among these metal oxides, manganese cobaltite (MnCo_2O_4) is especially interesting because of its unique properties such as environmental friendly, high capacity and nontoxicity, and it can be vastly studied in diverse zones including Lithium-ion batteries, adsorption, catalyst, etc. [16–18].

On the other hand, zeolites are introduced as a class of porous crystalline hydrated aluminosilicate of the elements of the alkali and alkaline-earth materials, and they have been utilized in many research fields such as environmental pollution, waste treatment process and catalyst [19–21]. Among

the various types of zeolite, Y-zeolite with FAU (Faujasite) structure has attracted more attention affiliated to their inner pore diameter of 12 Å and a large pore of 7.4 Å, high surface area, thermal stability and higher content of aluminum in its crystalline framework [22]. Due to these outstanding features, it can be chosen as a suitable candidate for the incorporation with MnCo_2O_4 NPs. Additionally, as an applying instrument for accurate measurements of radionuclides (α and β emitters), ultra-low level liquid scintillation counting (LSC) has been widely used for many monitoring and researches purposes. Low equipment necessity and the ease of required radiochemical preparations, make LSC as a plausible technique which can be employed even by laboratories with the paucity of special radiochemistry equipment and experience [8]. It is also notable when the removal experiments were fully completed, the appropriate volume of surface solution related to each of reaction containers was mixed with the cocktail and introduced to the LSC device and the relevant results were recorded. In the present research, the synthesis and characterization of $\text{MnCo}_2\text{O}_4/\text{NaY}$ as a novel nanocomposite adsorbent and its performance for effective removal and adsorption of Sr^{2+} from drinking water of Tehran city has been investigated and reported. The effects of adsorbent dose, pH, adsorbent type and contact time and the kinetics and thermodynamic reactions have also been studied in detail. However to the best of our knowledge, there has not been any study or report developing such adsorbent on the specified issue.

Experimental

Materials

Manganese nitrate tetrahydrate $\text{Mn}(\text{NO}_3)_2 \cdot 4\text{H}_2\text{O}$, cobalt nitrate hexahydrate $\text{Co}(\text{NO}_3)_2 \cdot 6\text{H}_2\text{O}$, aluminum trihydrate (H_6AlO_3), sodium silicate (Na_2SiO_3), sodium hydroxide (NaOH), nitric acid (HNO_3), ethanol ($\text{C}_2\text{H}_5\text{OH}$), acetone ($\text{C}_3\text{H}_6\text{O}$) and disodium ethylenediaminetetraacetate dihydrate ($\text{Na}_2\text{EDTA} \cdot 2\text{H}_2\text{O}$) were all purchased from Merck and Sigma Aldrich companies. The high-capacity cocktail OptiPhase HiSafe-3 (Wallac Oy, Turku, Finland) and deionized water were used throughout the research.

Instrumentation

To provide a better understanding of the morphology and elemental composition of the samples, a scanning electron microscope equipped with energy dispersive X-ray spectrometer (SEM-EDAX, HITACHI S-300N) was operated. The atomic force microscope (AFM) of Danish Micro Engineering (DME) Danish Micro Engineering (A/S DK-2730 Denmark) was also utilized and the further experiments were

carried out at room temperature. Further, the powder X-ray diffraction (XRD) patterns were recorded by operating a Philips X'pert Pro diffractometer equipped with $\text{CoK}\alpha$ radiation at wavelength 1.54056 \AA (30 mA and 40 kV) at room temperature. The corresponded data were gathered over the scope of 4° – 80° in 2θ with step mode of 2° min^{-1} . The IR spectra were scanned on a PerkinElmer model 2000 Fourier-transform infrared (FT-IR) spectrometer in the wavelength range of 400 – 4000 cm^{-1} employing KBr pellets. An ultra-low level liquid scintillation counting (LSC, Wallac Quantulus 1220) was operated for all measurements. The mentioned device is particularly designed for the measurement of very low level radioactivity by employing an anticoincidence active and a passive shield and also low background structural materials. Further, a pulse analyzer divides pulses originated from alpha and beta radiations into various output spectra. Also the sample processing frequency is enhanced with an automatic sample changer which provides measuring up to 60 samples consecutively [8]. Besides, an ultrasonic apparatus (UP100H; frequency of 30 kHz and 100 W output acoustic power) was utilized to prepare the samples.

Synthesis of MnCo_2O_4 NPs

The MnCo_2O_4 NPs were prepared by co-precipitation method. Typically, $\text{Co}(\text{NO}_3)_2 \cdot 6\text{H}_2\text{O}$ (1.5 g) as the source of Co^{3+} and $\text{Mn}(\text{NO}_3)_2 \cdot 4\text{H}_2\text{O}$ (1.0 g) as the source of Mn^{2+} ions were dissolved in deionized water (100.0 mL). This homogenous mixture was under steady stirring for 30 min at room temperature. Subsequently, NaOH aqueous solution (100.0 mL of 3.2 M) was gradually added to the precursor solution to reach pH of 11.0 along with ongoing stirring for 60 min. Eventually, the resulted precipitate was filtered, washed by the ethanol and deionized water for multiple times and dried at 350°C for 12 h.

Synthesis of NaY zeolite

The NaY zeolite was synthesized through a hydrothermal route. In brief, NaOH (50.0 g) and deionized water (30.0 mL) were added together and heated to 100°C under rigorous stirring. Afterwards, H_6AlO_3 (4.8 g) was suddenly introduced to NaOH solution. Then, the prepared solution (10.0 mL) was diluted with deionized water (30.5 mL) and NaOH (2.8 g) was dissolved in the mentioned solution (solution A). On the other hand, Na_2SiO_3 (11.0 g) was dissolved and mixed with deionized water (30.5 mL) containing NaOH (2.8 g) (solution B). Then, solution (A) was slowly added to solution (B) and the gained mixture was properly agitated for 30 min. The supplied mixture was poured into a Teflon-lined stainless steel autoclave and remained at 90°C for 8 h in an oven. The resulting crystalline powder was then filtered and washed with deionized water thrice until the pH

of the washing solution was equal to that of deionized water. Finally, the attained powder dried at 100°C .

Synthesis of $\text{MnCo}_2\text{O}_4/\text{NaY}$ nanocomposite

To fabricate the $\text{MnCo}_2\text{O}_4/\text{NaY}$ zeolite nanocomposite via the ultrasound assisted dispersion method, at first, pre-synthesized NaY zeolite was calcined at 350°C for 4 h. Then, MnCo_2O_4 NPs (0.2 g) was dispersed in deionized water (25.0 mL) with sonication for 60 min at room temperature. The NaY zeolite (2.0 g) was also added to the prepared suspension of the MnCo_2O_4 NPs and the outcome mixture was vigorously shaken for overnight. Consequently, the resulting product was filtered and further dried at 60°C for 8 h and calcined at 350°C for 12 h.

Sr^{2+} adsorption tests

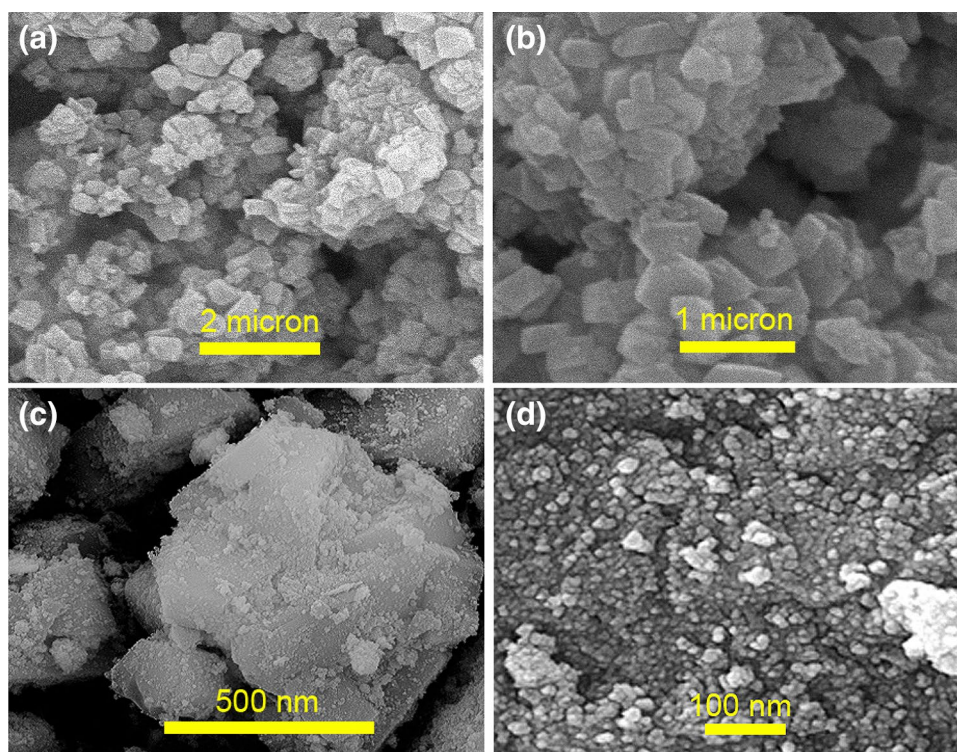
To investigate the adsorption-removal susceptibility of as-synthesized nanocomposite adsorbent toward Sr^{2+} (with initial source activity of 190.39 Bq), firstly, the value of 0.05–0.4 g of the $\text{MnCo}_2\text{O}_4/\text{NaY}$ was introduced to the drinking water (100.0 mL) of Tehran city. Next, the samples were stirred for time intervals of 60, 120, 180, 240 and 360 min by permutation the temperature between 298 and 328 K. All of the samples were then filtered and 5.0 mL of supernatant solutions were counted by the ultra-low level liquid scintillation counting (LSC) analysis for 300 min. To initiate the measurements by LSC, an adequate volume of each sample was poured into a vial and mixed homogeneously by scintillation cocktail (15.0 mL). 20.0 mL polyethylene vials (PEVs), Poly vial were applied to contain the mixed samples and the noted cocktail. To remove any probable dust or external pollution, the outside of each vial was cleaned precisely by acetone solvent. Moreover, to prevent the scintillation cocktail fluorescence, all of the PEVs were imposed in a dark shield and cooled for about 120 min.

Result and discussion

SEM

The evaluation of the surface morphology and crystalline size of the pristine NaY zeolite (Fig. 1a, b), $\text{MnCo}_2\text{O}_4/\text{NaY}$ zeolite nanocomposite (Fig. 1c) and pristine MnCo_2O_4 NPs (Fig. 1d) were determined via SEM as depicted in Fig. 1. The expected homogenous morphology of the NaY zeolite and further sphere-like shapes of the MnCo_2O_4 NPs which were sufficiently deposited on the NaY zeolite can be comprehensively described by SEM images. Looking crossly to the attained images, again it is confirmed that there is no sign of deformation or destructive impact related to the

Fig. 1 SEM images of: **a** and **b** pristine NaY, **c** $\text{MnCo}_2\text{O}_4/\text{NaY}$ and **d** pristine MnCo_2O_4



deposition stages on the crystallinity and morphology of the $\text{MnCo}_2\text{O}_4/\text{NaY}$ zeolite composite frameworks. The estimations revealed the average crystalline size of less than 12 nm for the MnCo_2O_4 NPs in the fabricated nanocomposite.

EDAX

The elemental composition of the synthesized $\text{MnCo}_2\text{O}_4/\text{NaY}$ zeolite nanocomposite (Fig. 2a) and pristine MnCo_2O_4 NPs (Fig. 2b), was investigated using energy dispersive X-rays (EDAX) analysis and the relevant outcome has been represented in Fig. 2. From the spectra, the presence of Na, O, Al, and Si elements in the $\text{MnCo}_2\text{O}_4/\text{NaY}$ structure is strongly acknowledged which corroborates the collected results from the XRD patterns. Also, the seven identified

peaks for each of Mn and Co in Fig. 2a spectrum clearly prove the presence of these elements in the $\text{MnCo}_2\text{O}_4/\text{NaY}$ nanocomposite structure. According to the provided data, the coexistence of MnCo_2O_4 with 18.7 wt% in the nanocomposite framework is explicitly corroborated.

AFM

To study the particle size and the morphology of the as-prepared $\text{MnCo}_2\text{O}_4/\text{NaY}$ (Fig. 3a) and pristine MnCo_2O_4 (Fig. 3b), the atomic force microscopy (AFM) were utilized and the resulted images represented in Fig. 3. Based on the AFM image (Fig. 3a), the mean particle size was estimated to be 12 nm for the MnCo_2O_4 NPs in the $\text{MnCo}_2\text{O}_4/\text{NaY}$.

Fig. 2 EDAX analyses of: **a** $\text{MnCo}_2\text{O}_4/\text{NaY}$ and **b** pristine MnCo_2O_4

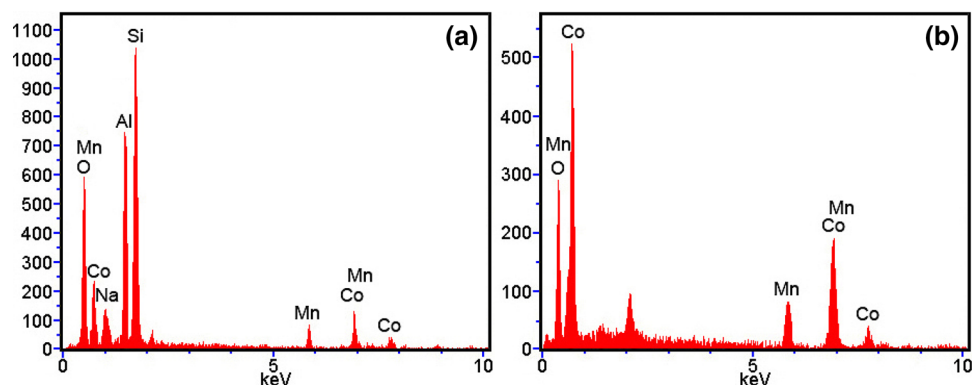


Fig. 3 AFM images of: **a** $\text{MnCo}_2\text{O}_4/\text{NaY}$ and **b** pristine MnCo_2O_4

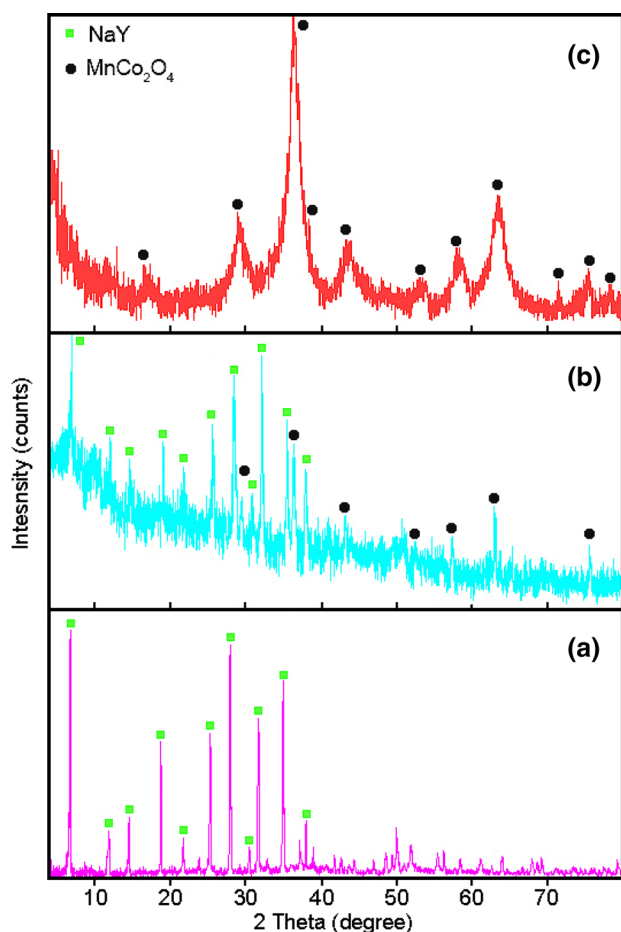
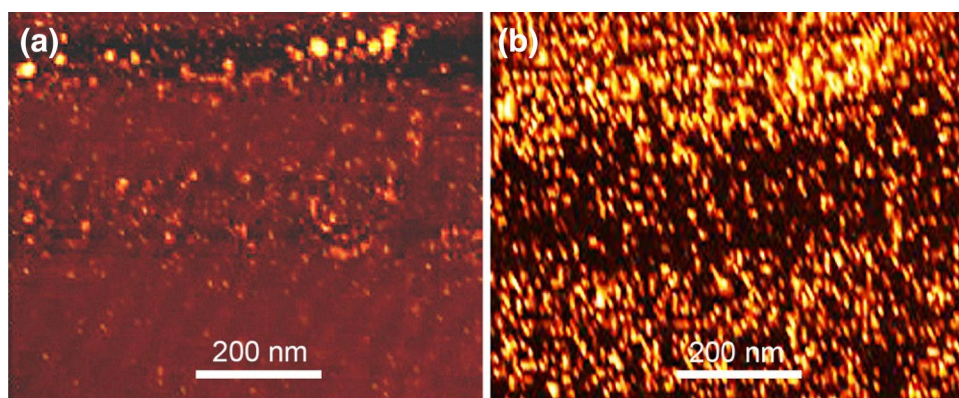


Fig. 4 XRD patterns of: **a** pristine NaY, **b** $\text{MnCo}_2\text{O}_4/\text{NaY}$ and **c** pristine MnCo_2O_4

XRD

The structural features of the prepared samples were analyzed by powder X-ray diffraction patterns. The related XRD patterns of the pristine NaY zeolite (Fig. 4a), $\text{MnCo}_2\text{O}_4/\text{NaY}$ zeolite nanocomposite (Fig. 4b) and pristine MnCo_2O_4 NPs (Fig. 4c) have been respectively

illustrated in Fig. 4. From these patterns, the major sharp peaks corresponded to two Y-zeolite emerged at 2θ values of 7.1502° – 35.3471° were created by the diffraction planes of (111) to (503), respectively. They were in good consistency with the defined values for the NaY zeolite with JCPDS Card No. 041-0118. The deposition procedure which was implemented in order to introduce the MnCo_2O_4 NPs to the framework of NaY zeolite to create $\text{MnCo}_2\text{O}_4/\text{NaY}$ zeolite nanocomposite caused no destructive effect on the zeolite structure. The deposition of the synthesized MnCo_2O_4 NPs as the guest materials on the NaY zeolite considered as the host material caused seven clear peaks which were observed at 2θ of 29.1428° , 36.1266° , 42.1001° , 53.1043° , 57.3451° , 64.4708° , and 75.1172° relating to the diffraction planes of (220), (311), (400), (422), (511), (440), and (533), respectively. Besides, during the deposition process of MnCo_2O_4 species, no characteristic peak referring to the impurities presence was identified in the provided patterns. Further, by using the well-known Debye–Scherrer formula (1) [23] the average crystalline size of the synthesized MnCo_2O_4 NPs deposited on the NaY zeolite was estimated:

$$D_{\text{XRD}} = \frac{K\lambda}{\beta \cos\theta} \quad (1)$$

In the represented formula, the average crystalline size is specified as D_{XRD} , K is the shape factor (0.94), the wavelength of $\text{CoK}\alpha$ radiation is shown as λ , the full width at half maximum (FWHM) of the considered diffraction peak is defined as β and θ is referred to the Bragg diffraction angle. Meanwhile, eleven peaks assigned to the pristine MnCo_2O_4 NPs appeared at scattering angles of $2\theta = 16.4062^\circ$, 29.1657° , 36.1428° , 37.4490° , 42.1002° , 53.1255° , 57.3719° , 64.4932° , 71.2517° , 75.1246° and 79.0194° relating to the diffraction planes of (111), (220), (311), (222), (400), (422), (511), (440), (620), (533), and (444), respectively which were in great consistency with those of MnCo_2O_4 NPs (JCPDS Card No. 20-1237). From the above mentioned equation, the average particle size for

MnCo_2O_4 NPs in the $\text{MnCo}_2\text{O}_4/\text{NaY}$ zeolite nanocomposite is calculated ~ 10 nm.

FTIR

The FTIR analysis was performed to study the functional groups of the prepared samples. Therefore, the affiliated spectra of the pristine NaY zeolite, $\text{MnCo}_2\text{O}_4/\text{NaY}$ zeolite nanocomposite and pristine MnCo_2O_4 NPs have been shown in Fig. 5. Considering the recorded spectra, it is deduced that the appeared peaks positions are nearly equivalent for those two Y-zeolite included samples. The bending vibrations of the insusceptible internal SiO_4 or AlO_4 tetrahedral units and plus double six rings (D6R) external linkage in the NaY zeolite structure caused the emerged peaks around 454 cm^{-1} and 573 cm^{-1} respectively. The external connection and internal tetrahedral symmetrical stretching vibrations make the peaks appear at about 711 cm^{-1} and 764 cm^{-1} respectively. Also, the observed peaks at 1019 cm^{-1} can be attributed to the external connection and also internal tetrahedral asymmetrical stretching vibrations. Moreover, the hydroxyl groups (O–H bonding and H–O–H bending) vibrations and plus segregated H_2O absorption bond in the NaY zeolite, lead to form peaks around 1645 cm^{-1} and 3565 cm^{-1} respectively.

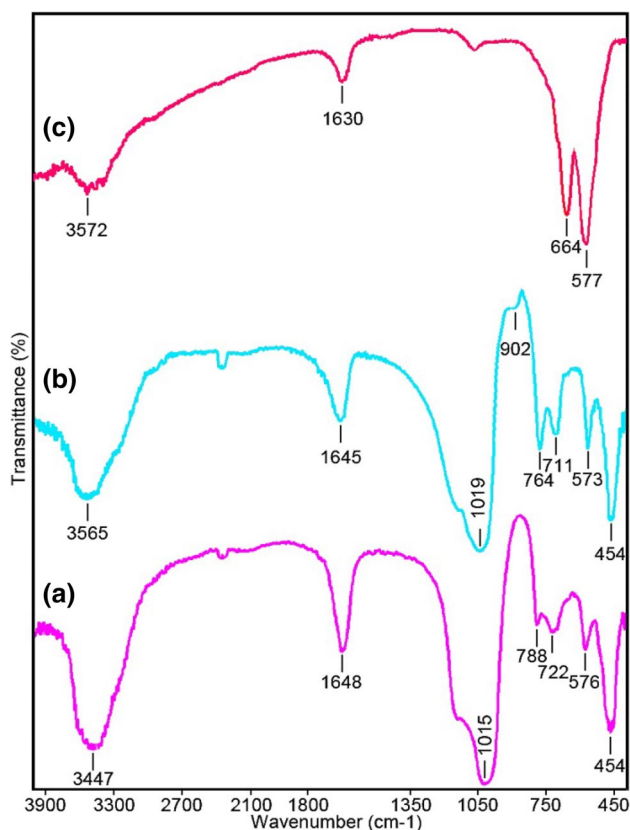


Fig. 5 FTIR spectra of: a pristine NaY, b $\text{MnCo}_2\text{O}_4/\text{NaY}$ and c pristine MnCo_2O_4

Based on the collected results from Fig. 5a, b, the deposition process had caused no tangible change or deformation on the zeolite framework as there has been no citable variation in the bonds of $\text{MnCo}_2\text{O}_4/\text{NaY}$ zeolite nanocomposite in comparison with those of NaY zeolite. Elsewhere, a bond of the M–O–Si and/or M–O–Al (M=Mn and/or Co) which is attributed to the deposited MnCo_2O_4 NPs in the structure of zeolite caused a new peak at 902 cm^{-1} as can be seen in Fig. 4b. Meanwhile, from the FTIR spectrum of pristine MnCo_2O_4 NPs in Fig. 5c, two peaks at 577 cm^{-1} and 644 cm^{-1} were due to the stretching vibrations of $\text{Mn}^{2+}\text{--O}$ and $\text{Co}^{3+}\text{--O}$ bonding respectively that confirms the formation of the spinel phase. Besides, the broad identified absorption peaks at around 1630 cm^{-1} and 3572 cm^{-1} are assigned to the adsorbed H_2O molecules in the MnCo_2O_4 structure.

Sr^{2+} removal and adsorption studies

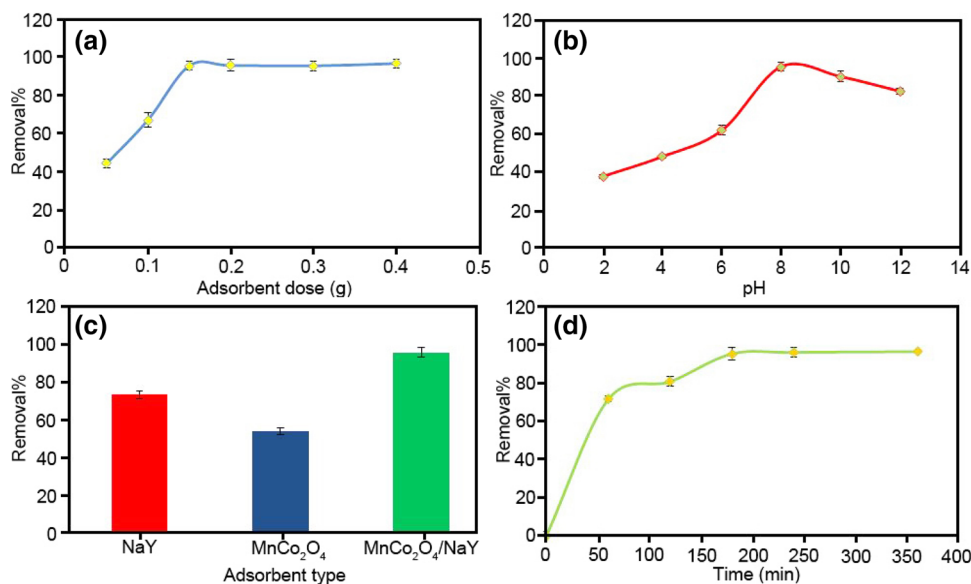
Effect of adsorbent dose

The use of the least dose of an adsorbent to approach the highest value of the adsorption and removal is of significant concern which makes the adsorbent creditable for further scientific investigations. In the present research, to recognize the optimized adsorbent dose for the removal of Sr^{2+} ions, the adsorption features of Sr^{2+} was assayed at range of $0.05\text{--}0.4$ g of $\text{MnCo}_2\text{O}_4/\text{NaY}$ nanocomposite. As can be inferred in Fig. 6a, the more the dose of used adsorbent, the higher the removal efficiency, till the point after which no more tangible changes is observed and the curve slope tend to a linear shape which insinuates to constant values. Ultimately, the value of 0.15 g was selected as an appropriate dose for $\text{MnCo}_2\text{O}_4/\text{NaY}$ nanocomposite to perform the high yield adsorption-removal process.

Effect of pH

The pH optimization experiments and its influence on the adsorption capability of prepared $\text{MnCo}_2\text{O}_4/\text{NaY}$ nanocomposite was investigated employing Sr^{2+} solution of 190.39 Bq at 298 K (optimized temperature) for 180 min. As demonstrates in Fig. 6b, the adsorption property of Sr^{2+} on the nanocomposite adsorbent was assayed at pH ranges between 2.0 and 12.0 . To approach the most sufficient selectivity and removal high efficiency, pH of 8.0 was assigned as an optimized value for the further modifications. Meanwhile, the solution pH was adjusted using 1.0 M solutions of NaOH and HNO_3 . After the sorption equilibrium was reached, the supernatant solution of Sr^{2+} were brought out and measured by the LSC device and the quantity of adsorbed-removed Sr^{2+} by nanocomposite adsorbent was computed. As a matter of fact, the hydroxyl groups originated from the interactions between hydrogen ions and an oxygen radical of the

Fig. 6 The effects of: **a** adsorbent dose, **b** pH, **c** adsorbent type and **d** contact time on the removal efficiency of Sr^{2+} ions



nanocomposite body reduces the matrix charge, which is accompanied with a descending route in the sorption susceptibility of zeolites regarding to the Sr^{2+} . Also, a higher sorption of the Sr^{2+} due to the pH increase, expresses that they are in an ionic state in the solution.

Effect of adsorbent type

The reactions of Sr^{2+} removal by varying adsorbent types ($\text{MnCo}_2\text{O}_4/\text{NaY}$ zeolite nanocomposite, pristine NaY zeolite and pristine MnCo_2O_4 NPs) were also investigated. All experiments were accomplished under similar conditions for those three adsorbents. Regarding to the gathered results from Fig. 6c, it is concluded that the highest removal efficiency of Sr^{2+} has been attained from the $\text{MnCo}_2\text{O}_4/\text{NaY}$ zeolite nanocomposite verifying the advantageous combination of NaY zeolite with MnCo_2O_4 NPs.

Effect of contact time

The influence of various time intervals on the adsorption-removal procedure of Sr^{2+} on the $\text{MnCo}_2\text{O}_4/\text{NaY}$ nanocomposite was examined. Figures 6d and 7 explains the difference of removal efficiency (%) versus shaking time and further the credibility of adsorption yield of Sr^{2+} ions on the synthesized $\text{MnCo}_2\text{O}_4/\text{NaY}$ nanocomposite adsorbent to the contact time. Therefore, the adsorption time was examined in the range of 60–360 min. As the time of reaction increased, the adsorption rate increased up to 180 min and after which remained in constant rate. To achieve the short time analysis with the highest yield of adsorption-removal, the time interval of 180 min was selected as an optimum value and more information have been represented in Table 1.

Adsorption kinetics study

The kinetic evaluations are accomplished for three main reasons: first, the determination of the concentration and temperature effects on the reaction rates, second, the examination of reaction rates under variant experimental conditions, and third, for assessment of the required time to approach the equilibrium during the adsorption process. Meanwhile, the adsorption kinetics investigation was carried out when the samples had been prepared by the addition of 0.15 g of $\text{MnCo}_2\text{O}_4/\text{NaY}$ nanocomposite at pH 8.0, in separate containers, at 298 K and particular time intervals. The adsorption value of Sr^{2+} ions at time t , q_t (mg/g), was computed by following Eq. (2) [24]:

$$q_t = (C_0 - C_t) \times \frac{V}{m} \quad (2)$$

where C_0 and C_t are known as the Sr^{2+} concentrations in the original solution and after passed time t , respectively. The volume of the solution V (L) and m (g) is corresponded to the used weight of the $\text{MnCo}_2\text{O}_4/\text{NaY}$ nanocomposite. The pseudo first and second orders, Intra particle diffusion and Elovich kinetic models were applied for the measurement of the adsorption kinetics of Sr^{2+} ions on the above specified adsorbent.

Pseudo-first-order model

The pseudo-first-order model assumes that the rate of versatility of the solute removal by reaction time is particularly assigned to versatility in glut concentration and solid uptake value via reaction time (3) [25]:

$$\log (q_e - q_t) = \log q_e - \frac{k_1}{2.303} t \quad (3)$$

Fig. 7 LSC spectra for the removal of Sr^{2+} ions on the $\text{MnCo}_2\text{O}_4/\text{NaY}$ nanocomposite at different contact times: (up) count versus channel and (down) count versus energy; under optimized conditions (adsorbent dose = 0.15 g, pH 8.0 and $T = 298\text{ K}$)

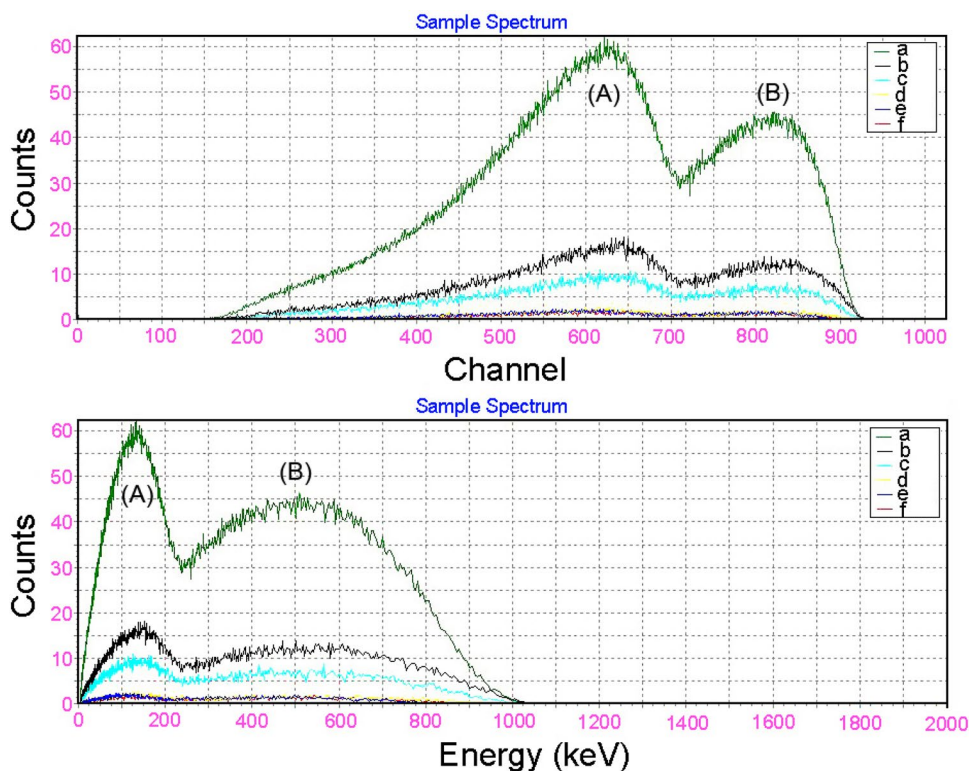


Table 1 The acquired results of the LSC analysis for the removal of Sr^{2+} on the $\text{MnCo}_2\text{O}_4/\text{NaY}$ nanocomposite under optimized conditions (adsorbent dose = 0.15 g, pH 8.0 and $T = 298\text{ K}$)

| Time (h) | Activity (Bq/sample) | CPM (A) | CPM (B) | Channel |
|----------|----------------------|----------------------|---------------------------|--------------------------|
| a | 0 | 190.39 | 43936.15 | 30417.32 |
| b | 60 | 53.29 (± 1.05) | 12297.69 (± 243.49) | 8513.78 (± 168.57) |
| c | 120 | 35.81 (± 0.58) | 8263.84 (± 134.70) | 5721.12 (± 93.25) |
| d | 180 | 8.09 (± 0.20) | 1866.93 (± 47.04) | 1292.48 (± 32.57) |
| e | 240 | 6.27 (± 0.20) | 1447.92 (± 47.34) | 1001.71 (± 32.75) |
| f | 360 | 5.59 (± 0.14) | 1289.99 (± 33.28) | 893.07 (± 23.04) |

where q_e and q_t (mg/g) are the adsorption capacity of Sr^{2+} ions at equilibrium and at time t , respectively, k_1 is referred to the pseudo-first-order constant (min^{-1}). The quantities of q_e and k_1 were determined from the intercept and slope of Fig. 8, respectively. Also, $\log(q_e - q_t)$ was depicted versus time interval, and if the first-order kinetics is credible, a straight line should be achieved with a slope of k_1 .

Pseudo-second-order model

A pseudo-second-order model was proposed for the adsorption of divalent metal ions on the sorbent particles as represented in following Eq. (4) [26]:

$$\frac{t}{q_t} = \frac{1}{k_2 q_e^2} + \frac{t}{q_e} \quad (4)$$

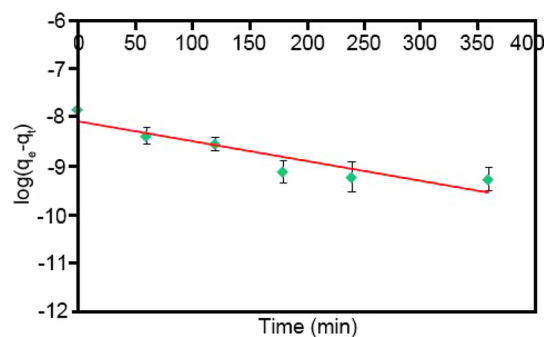


Fig. 8 The pseudo-first-order for the adsorption of Sr^{2+} on the $\text{MnCo}_2\text{O}_4/\text{NaY}$ nanocomposite

where q_e and q_t are referred to the amounts of Sr^{2+} (g mg^{-1}) at equilibrium and other time intervals. k_2 is the rate constant of the pseudo-second-order equation ($\text{g mg}^{-1} \text{min}^{-1}$). When

the pseudo-second-order is a sufficient expression, a pattern of $\frac{t}{q_t}$ against time (t) will provide a linear result with a slope of $\frac{1}{q}$ and an intercept of $\frac{1}{k_2 q_e^2}$ (Fig. 9). The adsorbed quantities (q) of Sr^{2+} were computed using the following Eq. (5) [27]:

$$q = (C_0 - C_e) \times \frac{V}{m} \quad (5)$$

where C_0 and C_e are corresponded to the initial and equilibrium concentrations of Sr^{2+} (g mg^{-1}) in the liquid phase, respectively. V is the volume of solution (L) and also m is the mass of adsorbent (g).

Intra particle diffusion model

Any adsorption procedure consists of different surface diffusion follows by intra particle diffusion. Basically, the liquid phase mass transport organized the adsorption process. The mass transport rate can be imparted as a function of the square root of time (t). As illustrated before, the intra particle diffusion model was explained by formula in below (6) [28]:

$$q_t = k_{ipd} t^{1.2} + C \quad (6)$$

At the noted formula, q_t refers the quantity of the adsorbed Sr^{2+} on the $\text{MnCo}_2\text{O}_4/\text{NaY}$ nanocomposite. k_{ipd} ($\text{mmol mg}^{-1} \text{min}^{-1}$) and t parameters are the intra particle diffusion rate constant and time, respectively. Also, C (mg mg^{-1}) is a constant that is affiliated to bounding layer thickness. Also, the value of correlation coefficient (R^2) was computed from the slope and intercept of the plot of q_t versus $t^{1.2}$ (Fig. 10).

Elovich kinetic model

The Elovich equation is demonstrated as can be seen in below (7) [29]:

$$\frac{dq_t}{dt} = \alpha \exp(-\beta q_t) \quad (7)$$

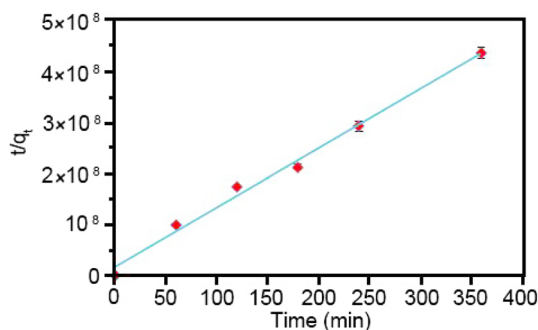


Fig. 9 The pseudo-second-order for the adsorption of Sr^{2+} on the $\text{MnCo}_2\text{O}_4/\text{NaY}$ nanocomposite

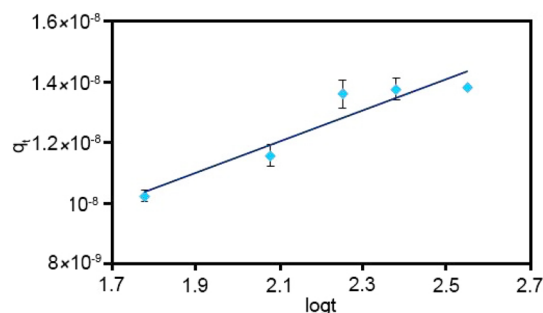


Fig. 10 The intra particle diffusion kinetics for the adsorption of Sr^{2+} on the $\text{MnCo}_2\text{O}_4/\text{NaY}$ nanocomposite

where α and β parameters are attributed to the initial sorption rate and desorption constant both (mg g^{-1}), respectively. If it is presumed that $\alpha\beta t \gg 1$, then the Elovich equation can be simplified. At the boundary conditions $q_t = 0$ at $t = 0$, the above specified equation converses to (8) (Fig. 11) [30].

$$q_t = \beta \log(\alpha\beta) + \beta \log t \quad (8)$$

The kinetic model accompanied with upper correlation coefficient (R^2) was assumed as the most relevant model. The kinetic factors of the Sr^{2+} adsorption on the $\text{MnCo}_2\text{O}_4/\text{NaY}$ nanocomposite have been depicted in Table 2. The obtained data proved that the adsorption of Sr^{2+} on the $\text{MnCo}_2\text{O}_4/\text{NaY}$ nanocomposite was followed by the pseudo-second-order model.

Thermodynamic studies

The adsorption and removal of Sr^{2+} on the $\text{MnCo}_2\text{O}_4/\text{NaY}$ nanocomposite was evaluated under certain optimized conditions. The corresponded results have been shown in Figs. 12 and 13. Furthermore, Fig. 13a depicts the effect of various temperatures on the removal of Sr^{2+} ions on the nanocomposite adsorbent surface. From the mentioned plot, it can be explicitly inferred that the adsorption of Sr^{2+} on the $\text{MnCo}_2\text{O}_4/\text{NaY}$ nanocomposite decreases by the gradual

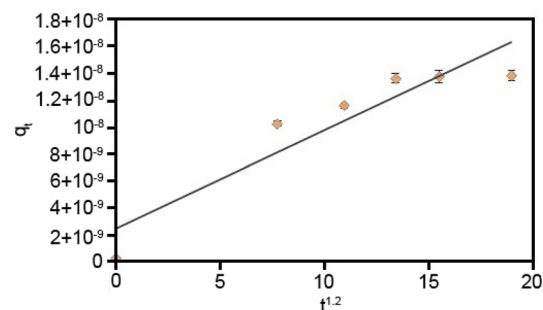
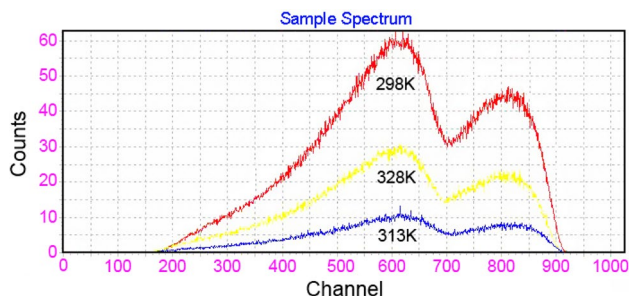


Fig. 11 The Elovich kinetics for the adsorption of Sr^{2+} on the $\text{MnCo}_2\text{O}_4/\text{NaY}$ nanocomposite

Table 2 The different kinetics model rate constants for the adsorption of Sr²⁺ on the MnCo₂O₄/NaY nanocomposite under optimized conditions (adsorbent dose = 0.15 g, pH 8.0 and T = 298 K)

| Kinetic model | Kinetic parameters | | R ² | Plot equation |
|--------------------------|---|--|----------------|---|
| First order | k ₁ (min ⁻¹) | 4 × 10 ⁻³ (± 9 × 10 ⁻⁵) | 0.8439 | y = -4 × 10 ⁻³ × -8.096 |
| Second order | k ₂ (g mg ⁻¹ min ⁻¹) | 10 ⁶ (± 2.3 × 10 ⁴) | 0.9921 | y = 10 ⁶ × +10 ⁷ |
| Intra particle diffusion | k _{ipd} (mmol mg ⁻¹ min ⁻¹) | 6 × 10 ⁻¹⁰ (± 1.4 × 10 ⁻¹¹) | 0.8637 | y = 6 × 10 ⁻¹⁰ × +2 × 10 ⁻⁹ |
| | C (mg mg ⁻¹) | 2 × 10 ⁻⁹ (± 4.7 × 10 ⁻¹¹) | | |
| Elovich | α | 0.9294 (± 2.2 × 10 ⁻²) | 0.8928 | y = 5 × 10 ⁻⁹ × +10 ⁻⁹ |
| | β | 5 × 10 ⁻⁹ (± 1.1 × 10 ⁻¹⁰) | | |

**Fig. 12** LSC spectra for the removal of Sr²⁺ on the MnCo₂O₄/NaY nanocomposite at different temperature

increase in the temperature. That is because of the loosening and eventual breaking of the formed bonds between Sr²⁺ ions and active sites of nanocomposite adsorbent as a consequence of raising the reaction temperature. To investigate the thermodynamic properties, several solutions were prepared in the range of pH 8.0 and then 0.15 g MnCo₂O₄/NaY nanocomposite added to each solution. Afterwards, the prepared samples were mounted on a stirrer and the solution stirred constantly at 298–328 K for 180 min, respectively. The quantity of adsorbed Sr²⁺ by the newly introduced adsorbent can be assigned by considering the difference between the initial and the equilibrium concentrations of Sr²⁺. To specify the process of spontaneous reaction, energy and entropy parameters should be noticed. Also, the coherency of distribution ratios on the temperature was studied. The correlation between K_d and ΔG⁰ variation in sorption has been shown in below (9) [31]:

$$\Delta G^0 = -RT \ln K_d \quad (9)$$

where R is the universal gas constant (8.314 J mol⁻¹ K⁻¹), T is the absolute temperature in kelvin (K) and K_d is the distribution coefficient. Gibbs free energy variation (ΔG⁰) can be also interpreted in terms of enthalpy variation (ΔH⁰) and entropy variation (ΔS⁰) as depicted in following Eq. (10) [31]:

$$\Delta G^0 = \Delta H^0 - T\Delta S^0 \quad (10)$$

Plus a new definition is attained by the integration of the equations 9 and 10 illustrated in below as Van't Hoff Eqs. 11 and 12 [32, 33]:

$$\ln K_d = -\frac{\Delta H^0}{R} \times \frac{1}{T} + \frac{\Delta S^0}{R} \quad (11)$$

$$K_d = \frac{q_e}{C_e} = \left(\frac{C_0 - C_e}{C_e} \right) \times \frac{V}{m} \quad (12)$$

where R is the universal gas constant (8.314 J mol⁻¹ K⁻¹), C₀ μmol/L parameter is the concentration in solution, C_e μmol/L parameter is known as the concentration in solution at equilibrium, V (L) is the solution volume, and m (g) represents the adsorbent mass. Meanwhile, both ΔH⁰ and ΔS⁰ of adsorption procedure can be delineated from the slope and the intercept of the linear fits which are obtained by plotting ln K_d versus 1/T respectively. Also, the negative values ΔG⁰ indicate that the adsorption procedure is spontaneous with linkage of Sr²⁺ ions to the nanocomposite adsorbent. According to the concluded data, the adsorption

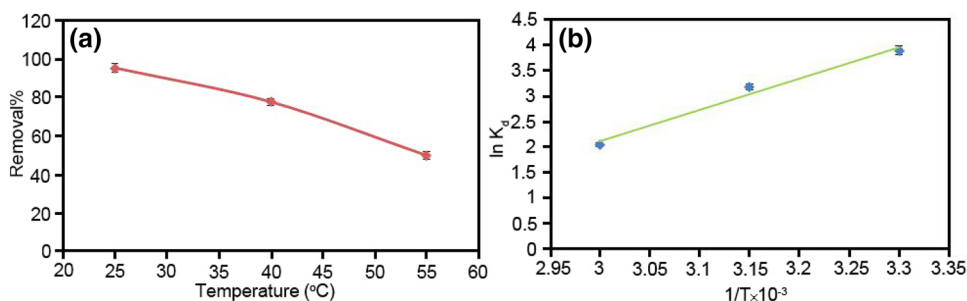
Fig. 13 Plots of: **a** Sr²⁺ removal% versus temperature and **b** Van't Hoff (ln K_d vs. 1/T) for the adsorption of Sr²⁺ on the MnCo₂O₄/NaY nanocomposite under optimized conditions (adsorbent dose = 0.15 g, pH 8.0 and contact time = 180 min)

Table 3 Thermodynamic parameters for the adsorption of Sr²⁺ on the MnCo₂O₄/NaY nanocomposite under optimized conditions (adsorbent dose = 0.15 g, pH 8.0 and contact time = 180 min)

| T (K) | ΔG^0 (kJ/mol) | ΔS^0 (J/mol K) | ΔH^0 (kJ/mol) | R ² | Plot equation |
|-------|--------------------------|---------------------------|---------------------------|----------------|------------------------|
| 298 | -9.6274 (± 0.2012) | 136.5923 (± 2.8547) | -51.3530 (± 1.0732) | 0.9837 | $y = 6.1767x - 16.428$ |
| 313 | -8.2388 (± 0.1721) | | | | |
| 328 | -5.5439 (± 0.1158) | | | | |

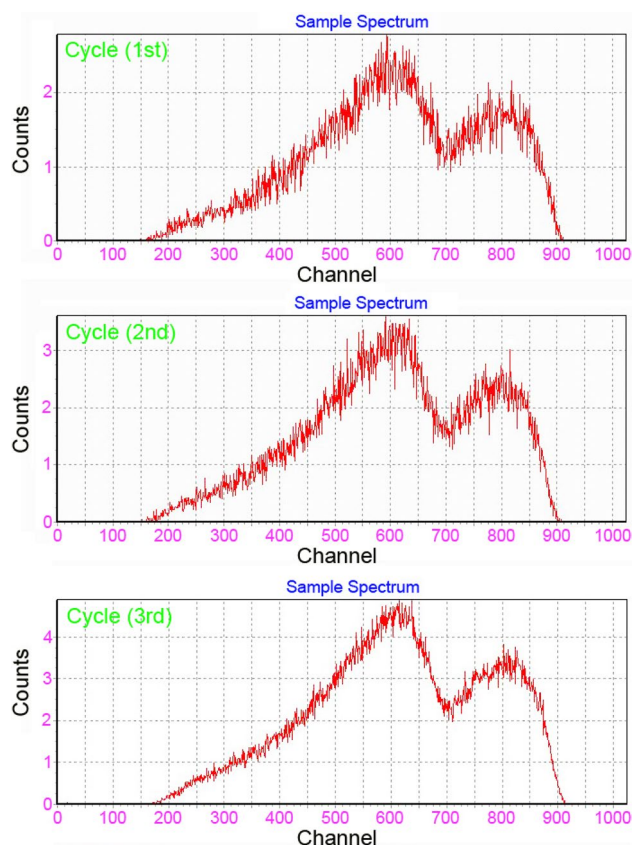
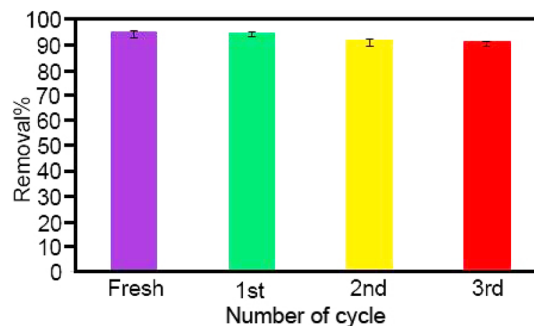
of Sr²⁺ on the MnCo₂O₄/NaY nanocomposite could be corresponded to a physic-chemical adsorption process ($\Delta H^0 = 51.3530$ kJ/mol). Thereupon, the enthalpy variance ΔH^0 following adsorption is negative which implies the exothermic nature of the adsorption. The entropy variances ΔS^0 of the system associated with the adsorption of Sr²⁺ ions on the MnCo₂O₄/NaY nanocomposite is recognized positive in all cases implying that no sensible change occurs in the internal structure of nanocomposite during adsorption of Sr²⁺. The drawing data of $\ln K_d$ versus $1/T$ has been depicted in Fig. 13b, and results are available in Table 3.

Reproducibility of the MnCo₂O₄/NaY nanocomposite

In order to investigate the reproducibility of the adsorbent for several times of reaction, the spent MnCo₂O₄/NaY nanocomposite was plunged in a solution of Na₂EDTA.2H₂O (0.2 M) and deionized water. Then this mixture was undergone stirring for 6 h at room temperature. After the washing process was fully accomplished, the accommodated Sr²⁺ ions were desorbed from the nanocomposite. Afterwards, the regenerated nanocomposite was further dried and employed for subsequent removal processes. Considering the results from several designed cycles, it is comprehended that a negligible diminution in the regeneration efficiency of the MnCo₂O₄/NaY nanocomposite occurs. However, using the mentioned nanocomposite for some consecutive cycles showed high removal efficiency for Sr²⁺ ions. As it has been illustrated in Figs. 14 and 15, the nanocomposite adsorbent was regenerated and applied for three sequential cycles and the removal efficiency of more than 91% was measured for all of those cycles.

The possible mechanism of Sr²⁺ adsorption

The characteristics including the presence of alkali and alkaline-earth metallic cations and porosity in zeolites framework accompanied with sufficient chemical and mechanical sustainability acquire high adsorptive, cation exchange, and catalytic features and further make them applying for use in vast fields of analytical approaches. Three major probable theories can be assumed for the adsorption mechanism of Sr²⁺ ions on the as-synthesized MnCo₂O₄/NaY nanocomposite adsorbent. (1) the intra porosity diffusion of Sr²⁺ ions

**Fig. 14** LSC spectra of the recovered MnCo₂O₄/NaY nanocomposite after three cycles in its adsorption reaction with Sr²⁺**Fig. 15** Reproducibility of the MnCo₂O₄/NaY nanocomposite under optimized conditions (adsorbent dose = 0.15 g, pH 8.0, contact time = 180 min and T = 298 K)

into the NaY zeolite framework which refers to the binding potentials of Sr^{2+} with active sites of NaY zeolite, (2) the ion exchange reactions among Na^+ , Mn^{2+} and Co^{3+} cations with negative charge balance of aluminum atoms and Sr^{2+} ions in aqueous solution, and (3) the van-der-waals or electrostatic forces of Sr^{2+} ions with negative charged hydroxyl groups and oxygen originated from nanocomposite framework.

Conclusion

In the current research, the $\text{MnCo}_2\text{O}_4/\text{NaY}$ (18.7 wt% of MnCo_2O_4) nanocomposite adsorbent was sufficiently synthesized and employed as an effective nanoadsorbent for the removal of Sr^{2+} ions from contaminated drinking water of Tehran city. The prepared nanoadsorbent was further characterized by different techniques including SEM, EDAX, AFM, XRD and FTIR, and the removal progression was measured and monitored via the LSC analysis. Various experimental conditions namely the adsorbent dose, pH, adsorbent type and contact time were impeccably surveyed and optimized. Also, the adsorbent quantity of 0.15 g, pH 8.0, contact time of 180 min, and temperature of 298 K were considered as the optimized conditions for subsequent experiments. The results showed that $\text{MnCo}_2\text{O}_4/\text{NaY}$ nanocomposite has the capability to perform the high yield adsorption-removal of Sr^{2+} ions from the aqueous matrix. The reaction kinetic information was investigated using pseudo first and second orders, intra particle diffusion and Elovich models. The adsorption kinetics of Sr^{2+} was desirably consistent to the pseudo-second-order kinetic model. More, thermodynamic study for the adsorption reaction was accomplished and the results confirmed that the increase of temperature has negative effect on the reaction efficiency as the reaction efficiency decreased when the temperature increased. Also the reproducibility experiments confirmed the significant applicability of the synthesized nanocomposite for high yield removal of Sr^{2+} ions for several cycles.

Acknowledgements The authors give their sincere thanks to the Lorestan University of Khorramabad, Iran for all sincere supports.

References

- Helal, A.I., Zahran, N.F., Amr, M.A., El-Lateef, A.A., Baster, I.I., Mohsen, H.T., Abbas, Y.: Ultratrace and isotope ratios analyses of some radionuclides by ICP-MS. *Radiochem. Acta* **92**, 369–374 (2004)
- Vonderheide, A.P., Zoriv, M.V., Izmer, V., Pickhardt, C., Caruso, J.A., Ostapczuk, P., Hillec, R., Becker, J.S.: Determination of ^{90}Sr at ultratrace levels in urine by ICP-MS. *J. Anal. At. Spectrom.* **19**, 675–680 (2004)
- Amr, M.A., Abdel-Lateef, A.M.: Comparing the capability of collision/reaction cell quadrupole and sector field inductively coupled plasma mass spectrometers for interference removal from ^{90}Sr , ^{137}Cs , and ^{226}Ra . *Int. J. Mass Spectrom.* **299**, 184–190 (2011)
- Sansone, U., Belli, M., Voitsekovitch, O.V., Kanivets, V.V.: ^{137}Cs and ^{90}Sr in water and suspended particulate matter of the Dnieper River-Reservoirs System (Ukraine). *Sci. Total Environ.* **186**, 257–271 (1996)
- Mohrbach, L.: Fukushima two years after tsunami—the consequences worldwide. *Atomwirtschaft* **58**, 152–155 (2013)
- Favre-Reguillon, A., Dungy, B., Lemaire, M., Chomel, R.: Synthesis and evaluation of resorcinol-based ion exchange resins for the selective removal of Cs. *Solvent Extr. Ion Exch.* **19**, 181–191 (2001)
- Krishna, M.V.B., Rao, S.V., Arunachalam, J., Murali, M.S., Kumar, S., Manchanda, V.K.: Removal of ^{137}Cs and ^{90}Sr from actual low level radioactive waste solutions using moss as a phyto-adsorbent. *Sep. Purif. Technol.* **38**, 149–0161 (2004)
- Sadeghi, M., Yekta, S., Ghaedi, H., Babanezhad, E.: Effective removal of radioactive ^{90}Sr by CuO NPs/Agclinoptilolite zeolite composite adsorbent from water sample: isotherm, kinetic and thermodynamic reactions study. *Int. J. Ind. Chem.* **7**, 315–331 (2016)
- Faghihian, H., Moayed, M., Firooz, A., Iravani, M.: Synthesis of a novel magnetic zeolite nanocomposite for removal of Cs^+ and Sr^{2+} from aqueous solution: kinetic, equilibrium, and thermodynamic studies. *J. Colloid Interface Sci.* **393**, 445–451 (2013)
- Ahmed, J., Ahmed, T., Ramanujachary, K.V., Lofland, S.E., Ganguli, A.K.: Development of a microemulsion-based process for synthesis of cobalt (Co) and cobalt oxide (Co_3O_4) nanoparticles from submicrometer rods of cobalt oxalate. *J. Colloid Interface Sci.* **321**, 434–441 (2008)
- Bhowmik, R.N., Rangana arajan, R.: Magnetic order and electrical conductivity scaling of the spinel oxide $\text{Mn}_{0.5}\text{Ru}_{0.5}\text{Co}_2\text{O}_4$. *Phys. Rev. B* **74**, 214417 (2006)
- Handley, R.C.O.: *Modern Magnetic Materials: Principles and Applications*. Wiley, New York (2000)
- Fang, X.H., Fang, F., Lu, Ch.H., Zheng, L.: Removal of Cs^+ , Sr^{2+} , and Co^{2+} ions from the mixture of organics and suspended solids aqueous solutions by zeolites. *Nucl. Eng. Technol.* **49**, 556–561 (2017)
- Ma, B., Oh, S., Shin, W.S., Choi, S.J.: Removal of Co^{2+} , Sr^{2+} and Cs^+ from aqueous solution by phosphate-modified montmorillonite (PMM). *Desalination* **276**, 336–346 (2011)
- Hosseini, F., Mozghan, I., Mohammad, M., Mohammad, G.M.: Preparation of a novel PAN-zeolite nanocomposites for removal of Cs^+ and Sr^{2+} from aqueous solutions: kinetic equilibrium, and thermodynamic studies. *Chem. Eng. J.* **222**, 41–48 (2013)
- Jin, R., Meng, Y., Ma, Y., Li, H., Sun, Y., Chen, G.: Hierarchical MnCo_2O_4 constructed by mesoporous nanosheets@polypyrrole composites as anodes for lithium ion batteries. *Electrochim. Acta* **209**, 163–170 (2016)
- Wang, K., Wu, X., Wu, W., Chen, W., Qin, L., Cui, X.: Synthesis of rambutan-like MnCo_2O_4 and its adsorption performance for methyl orange. *J. Therm. Anal. Calorim.* **122**, 653–663 (2015)
- Cao, X., Jin, C., Lu, F., Yang, Z., Shen, M., Yang, R.: Electrochemical properties of MnCo_2O_4 spinel bifunctional catalyst for oxygen reduction and evolution reaction. *J. Electrochem. Soc.* **161**, H296–H300 (2014)
- Rhodes, C.J.: Zeolites: physical aspects and environmental applications. *Annu. Rep. Prog. Chem. C* **103**, 287–325 (2014)
- Wang, S., Peng, Y.: Natural zeolites as effective adsorbents in water and wastewater treatment. *Chem. Eng. J.* **156**, 11–24 (2010)
- Azizi, S.N., Ghasemi, S., Kaviani, S.: Synthesis and characterization of NaX nanozeolite using stem sweep as silica source and application of Ag-modified nanozeolite in electrocatalytic reduction of H_2O_2 . *Biosens. Bioelectron.* **62**, 1–7 (2014)

22. Barlocher, C.H., Meier, W.M., Olson, D.H.: Atlas of Zeolite Structure Types, 5th edn. Elsevier, Amsterdam, (2001)
23. Debye, P., Scherrer, P.: The Scherrer equation versus the 'Debye-Scherrer equation'. *Phys. Z.* **17**, 277–283 (1916)
24. Sadeghi, M., Yekta, S., Ghaedi, H., Babanezhad, E.: MnO₂ NPs-AgX zeolite composite as adsorbent for removal of strontium-90 (⁹⁰Sr) from water samples: kinetics and thermodynamic reactions study. *Mater. Chem. Phys.* **197**, 113–122 (2017)
25. Lagergern, S.: About the theory of so-called adsorption of soluble substances. *K. Sven. Vetenskapsakad. Handl.* **24**, 1–39 (1898)
26. Ho, Y.S., McKay, G.: The kinetics of sorption of basic dyes from aqueous solution by sphagnum moss peat. *Can. J. Chem. Eng.* **76**, 822–827 (1998)
27. Agrawa, I.S.G., King, K.W., Fischer, E.N., Woner, D.N.: PO₄³⁻ removal by and permeability of industrial by products and minerals: granulated blast furnace slag, cement kiln dust, coconut shell activated carbon, silica sand, and zeolite. *Water. Air Soil Pollut.* **219**, 91–101 (2011)
28. Annadurai, G., Juang, R.S., Lee, D.J.: Use of cellulose-based wastes for adsorption of dyes from aqueous solutions. *J. Hazard. Mater.* **92**, 263–274 (2002)
29. Liang, S., Guo, X., Feng, N., Tian, Q.: Isotherms, kinetics and thermodynamic studies of adsorption of Cu²⁺ from aqueous solutions by Mg²⁺/K⁺ type orange peel adsorbents. *J. Hazard. Mater.* **174**, 756–762 (2010)
30. Gerente, C., Lee, V.K.C., Cloirec, P.L., McKay, G.: Application of chitosan for the removal of metals from wastewaters by adsorption-mechanisms and models review. *Crit. Rev. Environ. Sci. Technol.* **37**, 41–127 (2007)
31. Malkoc, E., Nuhoglu, Y.: Potential of tea factory waste for chromium(VI) removal from aqueous solutions: thermodynamic and kinetic studies. *Sep. Purif. Technol.* **54**, 291–298 (2007)
32. Nishiyama, Y., Hanafusa, T., Yamashita, J., Yamamoto, Y., Ono, T.: Adsorption and removal of strontium in aqueous solution by synthetic hydroxyapatite. *J. Radioanal. Nucl. Chem.* **307**, 1279–1285 (2016)
33. Merceille, A., Weinzaepfel, E., Barre, Y., Grandjean, A.: The sorption behavior of synthetic sodium nonatitanate and zeolite A for removing radioactive strontium from aqueous wastes. *Sep. Purif. Technol.* **96**, 81–88 (2012)